Wear 452–453 (2020) 203283

Contents lists available at ScienceDirect

Wear

journal homepage: http://www.elsevier.com/locate/wear

Wear mechanism evolution on brake discs for reduced wear and particulate emissions

Ran Cai [a], Jingzeng Zhang [a], Xueyuan Nie [a,*], Jimi Tjong [b], D.T.A. Matthews [c,**]

[a] Department of Mechanical, Automotive & Materials Engineering, University of Windsor, 401 Sunset Avenue, Windsor, Ontario, N9B 3P4, Canada
[b] Powertrain Engineering R&D Centre, Ford Motor Company, 1 Quality Way, Windsor, Ontario, N9A 6X3, Canada
[c] Department of Mechanics of Solids, Surfaces & Systems, Faculty of Engineering Technology, University of Twente, De Horst 2, Enschede, 7522LW, the Netherlands

ARTICLE INFO

Keywords:
Wear
Surface morphology
Ceramic coating
Brake
Non-exhaust emission

ABSTRACT

Brake disc wear contributes heavily to particulate matter as non-exhaust emission in the transportation sector. To tackle this issue, research on this topic has so far been directed at obtaining a hard and dense disc surface to reduce abrasive wear. The present research manipulates the disc surface morphology so that an adhesive transfer layer can be formed during sliding to protect the disc from wear. The designed interlocking surface was prepared using plasma electrolytic aluminating (PEA) process. A non asbestos organic (NAO) brake pad was used for tribotests. The results showed that the PEA-treated brake disc exhibited negligible wear because of the thin protective layer generated by the pad material transfer onto the PEA-treated cast iron. The dimple-like surface, produced through the PEA process, enhanced the bonding of the transfer layer due to mechanical interlocking. The coated surface increased the coefficient of friction of the disc to some extent. The surface also resulted in a reduced wear rate of the brake pad, highlighting the potential for the PEA process to enable reduced wear debris and thus non-exhaust emission through an altered wear mechanism in future brake disc applications.

1. Introduction

Up to 55% by mass of particulate matter (PM) emissions in the automotive sector come from non-exhaust traffic related emissions. Brake wear has been identified as one of the most significant contributors, being responsible for up to 21% of total urban traffic related PM_{10} emissions by mass [1–3]. About 50% of wear debris generated during braking become airborne while the rest is deposited on the road surface or is attracted to the vehicle [4–6]. Such particle emission has a strong adverse effect on air, water and ground quality. Additionally, some constituents of airborne particles have been recognized as having potentially dangerous effects on human health, such as weakening pulmonary antimicrobial immune defence, inducing heritable mutations, and affecting lung function [7–9]. Under growing health, safety and environment (HSE) concerns, manufacturers of both combustion engine and electric vehicles are demanding cleaner braking systems.

For brakes to function, the rotating discs and pads have to press against each other, causing wear and tear. During a braking event, the pad slides against the disc and transforms the vehicle's kinetic energy into thermal energy, generating not only mechanical abrasion but also large frictional heat with subsequent wear of both pads and discs. Humps on the surface of disc are pressed into the pad and debris is torn from the pad or sheared off from the disc. Some of this debris is ejected from the contacting interface. Other debris remains on the disc and pad surfaces and undergoes the cyclic deformation, crushing, fracture, and spalling or peeling. This debris can adhere onto the pad or disc base surface to form a friction film with a thickness of up to several hundred micrometers [10]. Commonly used brake pads are based on non asbestos organic (NAO), ceramic or semi-metal as friction materials, which have different characteristics of friction at low and high operating temperatures [1]. A semi-metallic brake pad often appears to have a higher average friction level and unfortunate propensity to generate more noise and dust. A ceramic brake pad is quiet with less dust generation; however, the ceramic pad is inferior to the NAO pad in frictional performance at low brake temperatures. The NAO pad does however show a higher tendency in brake fade if excessive heat is generated by aggressive braking. On balance of these properties, NAO pads are the preferred choice for millions of passenger vehicles.

There is an urgent need to reduce brake particle production and several approaches have been assessed to achieve reduced wear in a

* Corresponding author.
** Corresponding author.
E-mail addresses: xnie@uwindsor.ca (X. Nie), d.t.a.matthews@utwente.nl (D.T.A. Matthews).

https://doi.org/10.1016/j.wear.2020.203283
Received 24 January 2020; Received in revised form 14 March 2020; Accepted 30 March 2020
Available online 4 April 2020

variety of (high temperature) tribological contacts including thermal spraying or laser cladding. These can also be realized on the brake disc face [11–15]. A prime example is the Porsche Surface Coated Brake (PSCB) disc, which adopts a coating of tungsten carbide on a cast iron substrate. The reported results are remarkable, with claims that the surface modified disc lasts up to 30% longer than its uncoated counterpart, while a 90% reduction in brake dust is also reported [16]. However, to tackle wear and emission issues, the previous research has so far been emphasized on disc surface hardening or hard coatings based on a strategy applied to prevent abrasive wear. In the present work, an alternative surface modification is proposed for improved durability and environmental performance of a brake disc. Specifically, an interlocking surface is prepared using plasma electrolytic aluminating (PEA) process. PEA is a process very recently born from inspiration of the phosphating process and the plasma-electrolytic oxidation (PEO) process. The PEO process is commonly used to improve the corrosion resistance and tribological performance of aluminium (Al) and magnesium (Mg) alloys. Succinctly put, the PEO process utilizes a high electric voltage to induce the dielectric breakdown of a passive film on a metal surface. Subsequently, a ceramic oxide film will form on the surface. The ceramic oxide film can be tailored to provide desirable (thermo-) mechanical properties or for biomedical applications [17–22]. The PEA process is a plasma discharge-assisted process in which a composite (hercynite−alumina) ceramic coating is deposited on a ferritic surface from an aluminate-based solution [23]. Most significantly, the PEA-treated surface has a dimple-like interlocking morphology which is considered a key factor for transitioning the wear mechanism of a brake disc away from abrasive wear in this study.

Important aspect in testing of friction pairs for simulated brake contacts, are the frictional response to pad/disc, the wear mechanisms and the wear rates. In order to assess these tribological performance aspects of brake materials/friction pairs, generally one has a choice between a pin-on-disc (PoD) tester and a dynamometer. Recently, Federici et al. [24] provided a comparative case study for friction pairs of NAO brake pad materials in contact with pearlitic cast iron, similar to the reference situation in our study thus. In that critical comparison, the authors compare both the PoD and dynamometer test set-ups in dry sliding conditions and conclude importantly that the specific wear coefficients between the PoD and dynamometer tests were “proportional to the corresponding values obtained with the PoD at room temperature” [24]. In addition, similar friction values, wear mechanisms and limited disparity between friction layers produced in both tests are reported at room temperature. In this research, we focus on “cold” braking conditions and therefore here also consider tribo-testing by pin-on-disc methodology, a decision supported by the aforementioned research. Specifically, tribological testing was performed to ascertain the wear and friction performance of the PEA-treated and untreated cast iron materials in a simulated pad disc contact. To achieve this, a commercial NAO pad material was selected as the counterbody to the treated and untreated samples. The reason for this was due to its expected superior friction performance compared to ceramic brake pads at room temperature [1,25]. The difference in wear mechanisms between a PEA-treated and untreated discs was investigated. In addition, the debris productions caused by the treated and untreated disc are compared by virtue of analysis of the wear rates.

2. Experimental details

Gray cast iron (ASTM A247) was cut into 3 mm thick coupon samples with a diameter of 25.4 mm. The cast iron coupon discs were treated using the PEA process. During the PEA process, the cast iron sample was immersed into an electrolytic solution and biased with negative voltage. The electrolyte contained 15% ~ 20% sodium aluminate. The pulsed DC power supply was employed with a 40% duration of 1000 Hz. The samples were treated for 15 min at current density of 0.15 A/cm^2. A cooling system maintained the electrolytic solution temperature around

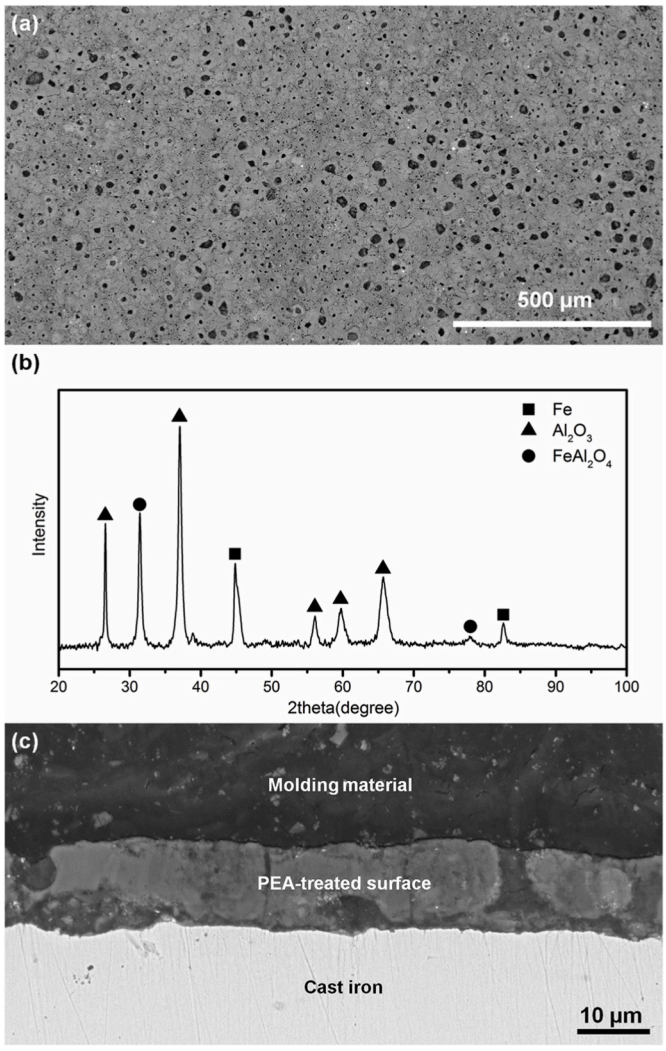

Fig. 1. (a) SEM images showing surface morphology of lightly polished PEA-treated surface; (b) XRD pattern of a PEA-treated surface on cast iron; (c) SEM images showing cross section of PEA-treated cast iron.

300 K. The PEA process has been reported previously described in detail [23]. After the process, we lightly polished the PEA-treated samples and cleaned them with compressed air and acetone. A scanning electron microscope (SEM) was used to observe the surface morphology of the PEA-treated surface and the elements of which were analyzed under an energy dispersive X-ray detector (EDX). The phase structures of the treated sample were investigated using an X-ray diffractometer (XRD) with Cu Kα radiation. XRD measurements were made from 20 to 100° 2 theta. Both the surface roughness and surface profiles were measured using a Mitutoyo surface profiler SJ201P. The hardness of the PEA-treated samples and the untreated cast iron samples was measured by Vickers hardness tester (Wilson VH1102). The tests were performed in a pin-on-disc tribometer to measure coefficients of friction (COF) of the treated and untreated brake discs. The tribometer is enclosed by a transparent plastic box. In this test, the pad to disc contact pair is replaced by pin and cast iron coupon sample. The pins worked as tribological counterparts were cut out of a commercially available NAO brake pad and machined into cuboid samples (5 mm × 5 mm × 10 mm) in which the square sides (5 mm × 5 mm) were the testing contact areas. The elemental distribution of the NAO pad materials was analyzed through an EDX. The pin-on-disc tribometer ran with a constant applied normal force of 20 N resulted in 0.6–0.9 MPa contact pressure which was similar to that of a normal braking operation [26]. The ambient air

Table 1
Typical surface properties of the samples before and after tribotests.

Sample	Material	PEA-treated surface	Cast iron
Polished surface	R_a (μm)	2.33	0.15
	R_{pk} (μm)	0.72	0.10
	R_{vk} (μm)	3.26	0.45
	Hardness (HV)	795	310
Wear track	R_a (μm)	1.65	0.29
	R_{pk} (μm)	0.76	0.09
	R_{vk} (μm)	3.95	1.14

temperature was at a room temperature of 297 K and the relative humidity was around 50–60% during the tests. The sliding speed was 0.05 m/s to simulate cold friction of a brake system at low temperature. The number of testing rotations for each test was 4000 (equivalent to 50 m sliding distance), during which the COF was recorded. After the tests, the sectional profiles of the wear tracks were obtained using the Mitutoyo surface profiler, and the wear loss was calculated based on the cross-sectional area multiplied by the circumference of the wear track. The wear rate is a wear loss per unit load and sliding distance. For a better comprehension of the wear and friction mechanism, the SEM and EDX were again utilized to study the surface morphology and elemental compositions on the wear tracks of treated and untreated cast iron samples.

3. Results and discussion

3.1. PEA-treated surface and pad material

Brake discs are commonly made of gray cast iron due to its high thermal conductivity, low cost and easy casting. Fig. 1a shows the surface image of the PEA-treated gray cast iron disc with a ceramic coating. The treated surface topography exhibits a characteristic dimple-like morphology with a porosity of 10–12%, while Fig. 1b shows the same surface's XRD pattern. The XRD data reveals the main constituent phase of surface coating is Al_2O_3 phase, coupled with a smaller fraction of $FeAl_2O_4$. Iron (Fe) peaks are present due to the reflections from the cast iron substrate. Fig. 1c presents the cross section of the PEA-treated cast

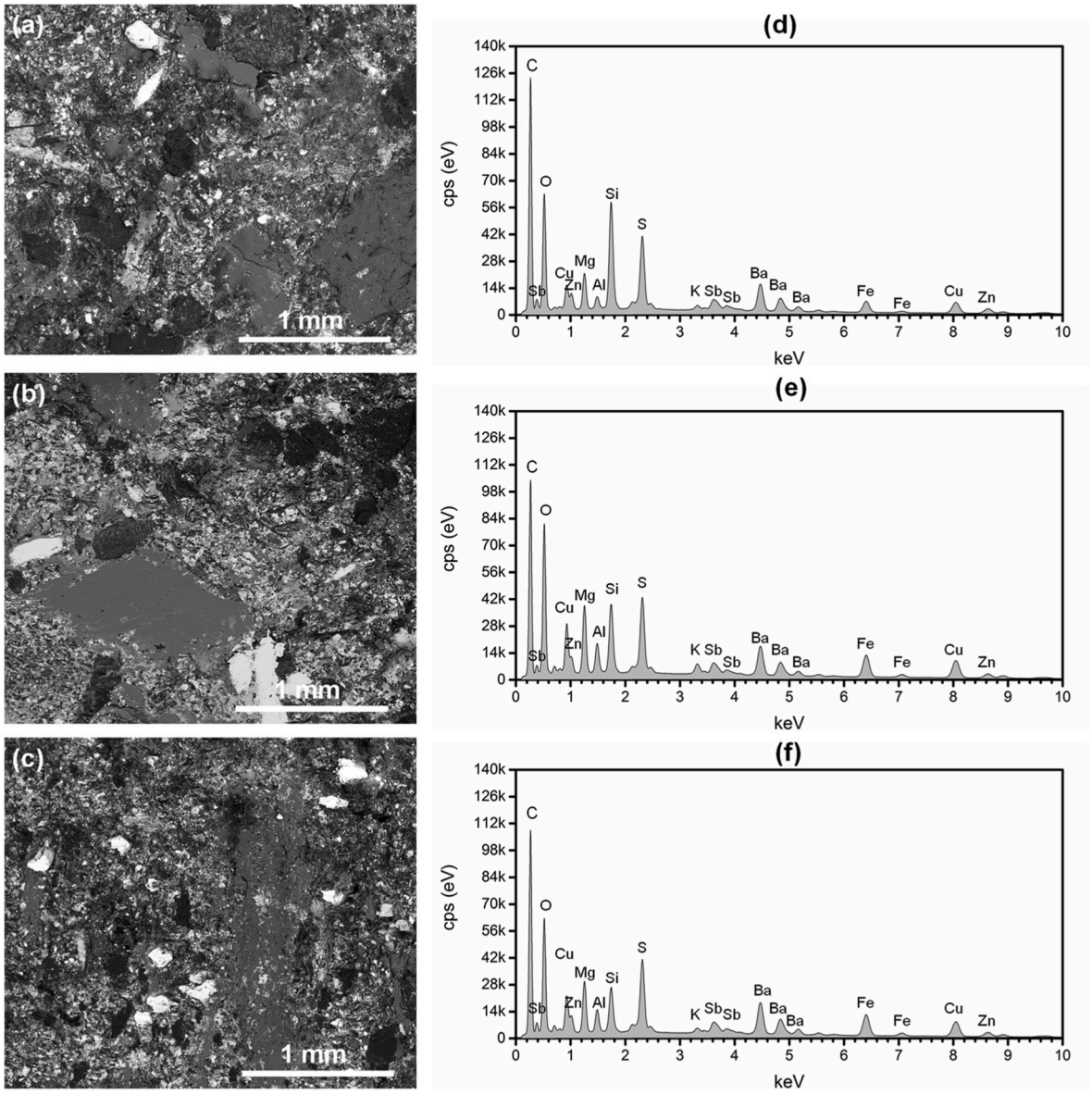

Fig. 2. SEM images and EDX of brake pads under different testing conditions: (a, d) original pad surface; (b, e) sliding on cast iron; (c, f) sliding on PEA-treated cast iron, respectively.

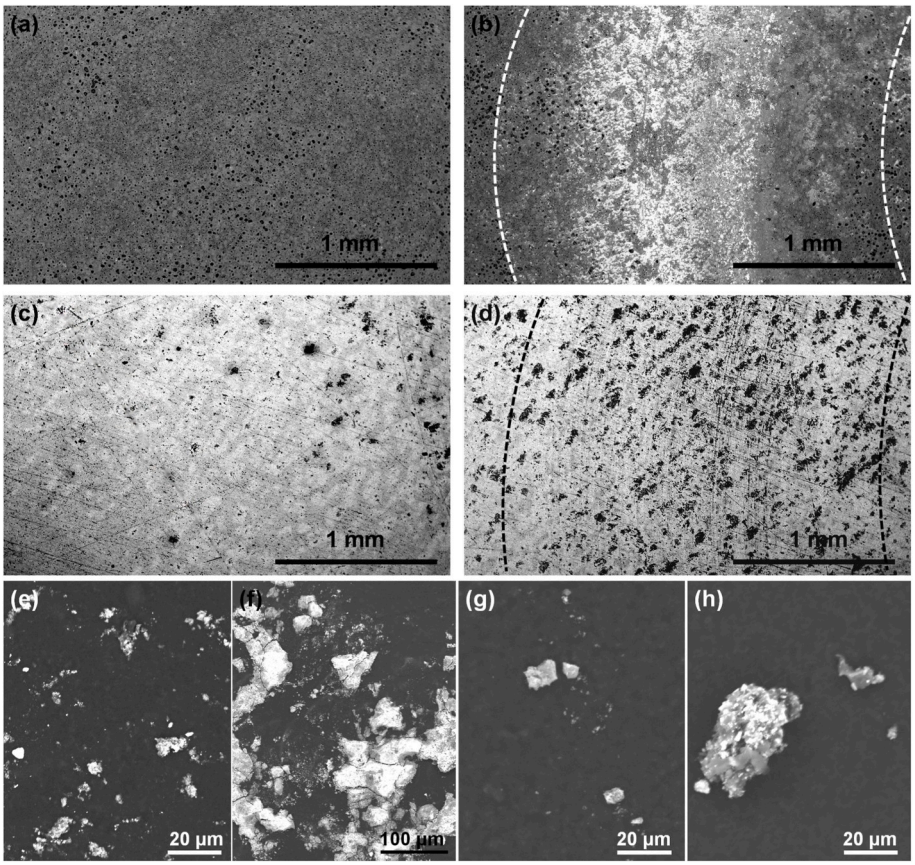

Fig. 3. SEM images: PEA-treated surface - (a) original polished and (b) wear track after test; untreated cast iron - (c) original polished and (d) wear track after test; wear debris collected from (e, f) treated and (g, h) untreated discs.

iron, showing the coating includes dense ceramic microstructures and pores. The coating thickness is 15–20 µm. The phase $FeAl_2O_4$ identified in the XRD analysis indicates that there is a metallurgical bonding between the PEA coating and the cast iron substrate [25]. Table 1 lists the average Vickers hardness of both the PEA-treated surface (795 $HV_{0.05}$) and the untreated cast iron (310 $HV_{0.05}$). The treated surface was 2–3 times harder than the untreated one. The cross-sectional hardness of the PEA-treated surface was reported to be in a range of 750–800 HV, depended on the locations away from the surface [23]. These results are in line with results reported in the previous study [23].

NAO is one of the commonly used brake pad types in passenger vehicles as its friction materials are less abrasive, have excellent noise, vibration and harshness (NVH) behavior and cause lower disc wear than other pads. Fig. 2 presents SEM images and elemental distribution maps of the NAO pads before and after the tribotests. The NAO pad in this study contains many friction materials which play different roles in the brake system. Depending on their specific roles, the friction materials are divided into five main categories: binders, reinforcing fibers, fillers, frictional additives or lubricants, and abrasives [1]. Binders are usually made of modified phenol-formaldehyde resins and hold the components of the brake pad together to ensure the structural integrity of the pad under mechanical and thermal stress [1]. Of the elements detected in the EDX mapping, copper (Cu) is present as Cu fibers and these are an example of reinforcing fibers. Such fibers increase both the thermal conductivity and mechanical strength of the material. Barium sulphate (Ba and S) and antimony sulphate (Sb and S) act as fillers in friction materials. Graphite (C) acts as lubricant to lower the friction coefficient. An unexpectedly high friction may cause overheating of a brake system and the graphite addition aims thus to combat this phenomenon. Iron (Fe) oxide, magnesium (Mg) oxide, silicon (Si) oxide and vermiculite (Si, Mg, Al, K and Fe containing mineral) are used as abrasives: iron oxide for regulating the coefficient of friction and increasing cold friction, magnesium oxide and silicon oxide for increasing the friction coefficient, and vermiculite for noise reduction. The chemical compositions of the brake pad surfaces were quite similar to each other before and after the tribotests, irrespective of the countermaterial. That is to say, the pad after testing against treated (Fig. 2e) or untreated cast iron (Fig. 2f) had almost the same EDX spectrum, which suggests that there was no material transfer from the PEA-treated surface or the cast iron surface to the pad material.

3.2. Surface morphology of wear tracks

The surface morphology of the wear tracks after tribotesting is shown in Fig. 3. The surfaces have been characterised by their average Roughness (R_a), their Reduced Peak Height (R_{pk}) and Reduced Valley Height (R_{vk}) values in order to quantify the surface topography. The results of these measurements, taken both before and after tribological testing, are shown in Table 1. The mildly polished PEA-treated surface (Fig. 3a) is characterised by higher roughness values than the untreated polished original cast iron (Fig. 3c). This can be attributed to the dimple-like PEA-treated surface. Fig. 3b shows that a thin film formed and attached on the treated surface in the wear track (bright areas) during the pin-on-disc tribotest, while no material build-up was identified on the cast iron sample. This tribo-contact was instead characterised by scratch marks in the wear track (Fig. 3d), indicating typical abrasive wear. It can be stated therefore that the dimple-like surface promotes the formation of a transfer layer from the brake pad, in a manner similar to compaction galling [27], while the pore-free surface of the gray cast iron, combined with the free carbon (graphite) prevents material sticking [28]. The chemical compositions of the respective tribo-tracks were characterised using EDX. Large amounts of oxygen were

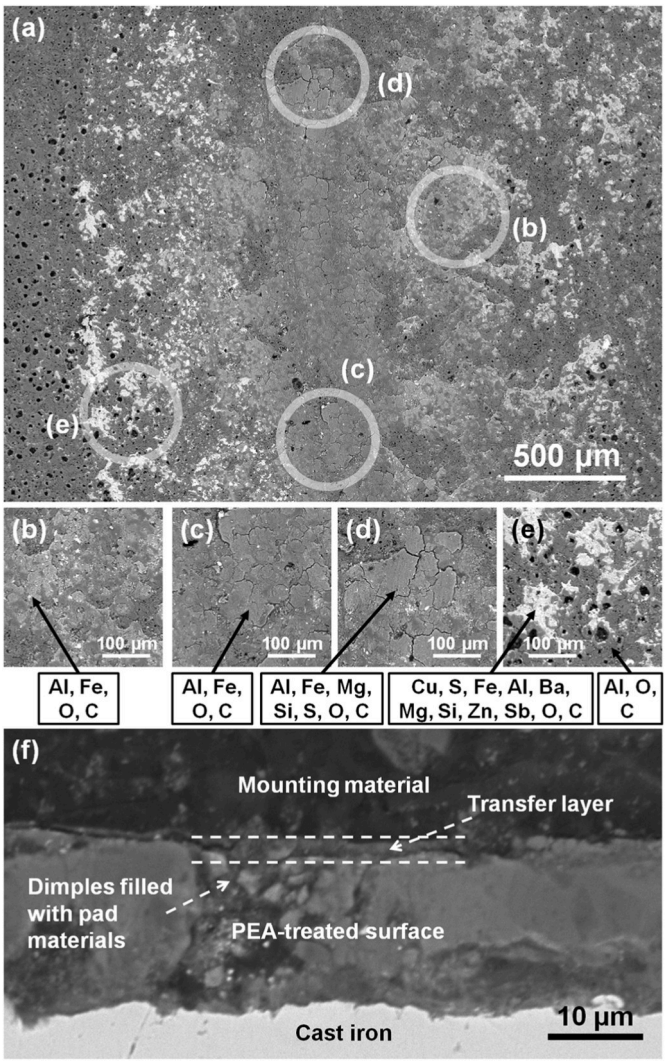

Fig. 4. SEM images showing: (a–e) surface morphology and related elements detected in the wear track of PEA-treated surface after testing; (f) cross-sectional wear track on the PEA-treated surface after the tribotest.

identified in the wear track of the untreated cast iron sample. It is reasonable to postulate that this oxidation was the result of frictional heat produced during sliding [28]. The EDX mapping identified increased dark areas in Fig. 3d compared to Fig. 3c as carbon, which was believed come from the pad through material transfer.

From Table 1, it can be seen that the characteristic roughness values of the treated surface are lower following the tribotests than prior to testing. That is, the surface becomes smoother within the tribological contact. We attribute this loss of roughness not to material loss or asperity flattening [20], but in fact due to the aforementioned material transfer. This also supports a hypothesis that debris build-up in the dimples of the treated sample will lead to local contact areas for the initiation of material transfer due to the galling induced overlayer [25] as will be discussed in more detail hereafter. On the other hand, the surface of the untreated cast iron sample became rougher following the tribotest. It is particularly interesting to note that the R_{vk} value increased greatly and this is attributed to the scratch marks identified previously (Fig. 3d). Fig. 3e–h shows the particle matters collected from the wear track surfaces at the early testing stage of 5 m sliding distance to visualize the particle size generation in the early contact phase. The particle collection is achieved through pressing SEM conductive carbon tapes on the wear tracks where the particles were picked up by the tapes. When the wear process proceeds for longer than 5 m sliding distance, the increased number of particles are already found to compact together, which in turn also makes observation of individual particles difficult. Fig. 3e and f presents images of the wear particles obtained from the PEA-treated cast iron surface. For the case of the treated cast iron disc, $PM_{2.5}$ and PM_{10} wear debris can be seen in Fig. 3e on the one hand. On the other hand, a significant portion of large wear debris has a particle size of 100–200 μm (Fig. 3f). The wear debris collected from the wear track of the untreated cast iron disc appears to have both $PM_{2.5}$ and PM_{10} particles (Fig. 3g). The particles can be as large as 20 μm (Fig. 3h) which was much smaller than the case in Fig. 3f. It is noteworthy that the more particles shown in Fig. 3e vs. Fig. 3g are due to collective behavior of dimple-like PEA-treated surface. In this case, the dimples act as reservoirs (having sizes of 1–50 μm as shown in Fig. 1a) and accommodate the fine particles to reduce airborne emission. After the stable transfer layer was formed, the wear particle sizes increased before the non-exhaust emission could occur. The large size and local compaction of PM seen in the case of PEA treated surfaces would cause less harm to human health [2,8,29]. We can also confer that the small wear debris on the untreated cast iron disc was generated from both the worn pad friction materials and the disc itself and then centrifugally ejected from the wear track, which is the reason why the fewer particles were picked up by the SEM carbon tape as shown in Fig. 3g and h, and also indication of a higher airborne emission.

To address our previously mentioned hypothesis on the wear mechanisms involved in the sliding of the treated sample against a NAO pad, we consider in Fig. 4a detailed electron microscopy analysis of the sample's wear track. While the transfer layer is not homogeneous under high magnifications, it can be seen to cover the original treated surface and fill the pores on the surface, as highlighted for example in the area of circle (b) in Fig. 4a. The thin layer appears to be well adhered dimpled surface, mostly likely due to mechanical interlocking where the material collects in the surface dimples initially as local islands (Fig. 4b). As mentioned, the transferred layer is not homogeneous, with some areas being thicker than others, with a secondary transfer layer apparently developing over the first transfer layer. This supports our hypothesis that the build-up takes the form of compaction galling. Other morphological features, such as cracks (Fig. 4c) and local spalling (Fig. 4d) are identified in the second layer. Furthermore, morphological variations are also identified transverse to the sliding direction. These differences and inhomogeneities can be related to the uneven distributions of friction materials in the brake pad (Fig. 4e, see also Fig. 2) which is reflected in the non-uniform development of the transfer layer – an observations supported also by discrepancies in both surface morphology and chemical compositions at different locations of the disc material surface (Fig. 4). Fig. 4f is a cross-sectional SEM image of the wear track on the PEA-treated surface after the tribotest, which also shows existence of the transfer layer on the top of the treated surface. It should be noted that surface topology of the transfer layer varied only in a few micrometers range approximately indicated by R_{vk} of the wear track on the PEA-treated surface in Table 1, which did not cause vibration and noise during the tribotest.

3.3. Tribological behaviors

Fig. 5a relays the dynamic coefficients of friction (COFs) for samples treated by the PEA process as well as the untreated gray cast iron variants. It is evident that the coefficient of friction for the treated sample is higher than the bare cast iron. The COFs of both test samples increased during the run-in period, and then gradually reached a stable level. When the friction reached a steady state, the COFs were 0.31–0.32 for the PEA-treated cast iron and 0.25–0.26 for the untreated cast iron. The average COFs obtained from 3 repeated tests were 0.31 ± 0.04 and 0.25 ± 0.07 for treated and untreated discs, respectively.

After the test program was completed, a digital dial indicator was used to determine the height variation of the brake pad sample and this data was then used to calculate the wear of the pads. Fig. 5b reveals

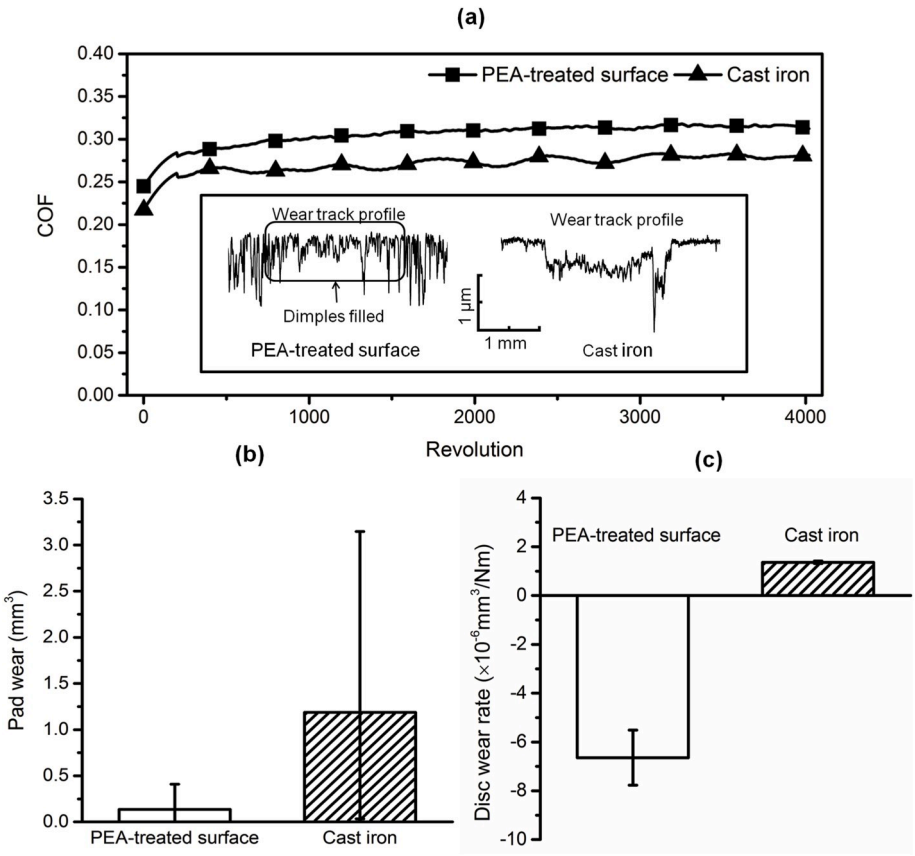

Fig. 5. (a) Coefficients of friction with insert of sectional profiles of wear tracks, (b) wear of the brake pads, and (c) wear rates of PEA-treated and untreated discs.

these results as the wear of the brake pads after comparative sliding distances against the various disc surfaces prepared in this study. Despite the differences in surface morphologies seen in section 3.2 and the related observation that material is transferred to the PEA-treated sample during sliding, the PEA-treated cast iron is actually found to result in a significantly lower (up to 75%) brake pad wear, compared to bare cast iron. In Fig. 5b, the large measurement error calculated from tribotests repeated at least 5 times was caused by uncertainty during each of the repeated tests when dynamic formation or detachment of a transfer layer (or so-called secondary plateaus [1]) on the pad surfaces arbitrarily occurred. Some of the wear debris was compacted and attached back to the pad contacting surfaces before emitting to the air.

To increase the precision of measurements for the wear rates of the treated and untreated cast iron discs, each tribotest was repetitively performed four times. In other words, 50 m sliding distance (i.e. 4000 revolutions) was repeated four times on the same wear track before the wear tracks were measured using a surface profilometer. By doing so, the wear tracks were obviously shown from their surface profile curves. This also increases the certainty of the wear measurements. Such a tribotest series was repeated at least 3 times on different disc surfaces against virgin pad surfaces for both untreated and PEA-treated discs. The average wear rate of the untreated cast iron disc is 1.36×10^{-6} mm^3/(N·m), while the wear rate of PEA-treated cast iron is negative, as shown in Fig. 5c where the error bars are also given. The negative value indicates that a transfer layer was formed on the PEA-treated surface, which confirms the observation in Fig. 4. The wear profiles (insets Fig. 5a) suggest that the negative wear rate is predominantly due to the material transfer to the surface dimples, resulting in a stable surface layer. Subsequently, the transfer layer thickness hardly increased with sliding distances; newly generated wear debris from the brake pad is added to the disc's transfer layer through compaction galling as fine PM and sequentially released to the air as large PM at a similar rate in terms of mass or volume loss [25].

Recollecting the previous observations, we can relate this to be the result of a disparity in friction mode. More specifically, in the tribological contacts investigated here, the cast iron material undergoes an abrasive-like friction sliding while the PEA-treated surface produces a contact characterised by adhesive-like friction sliding combined with compaction galling. The SEM images in Fig. 2, showing the surfaces of the brake pad segments before and after the sliding tests, demonstrate that after being tested against the PEA-treated surface, the pad has a smoother surface (Fig. 2b) compared to not only the original pad (Fig. 2a) but also the pad tested against the untreated cast iron disc (Fig. 2c). Small surface cracks can be seen on the pad after it was tested against untreated cast iron. Thus, we can conclude that the effect of PEA-treated surfaces lead to a less aggressive tribological degradation of the NAO pad.

These observations of course have practical implications in materials and surface design in brake tribology and can pave the way for further developments. We know that there are two main types of friction mechanism associated with disc-pad contacts, namely abrasive friction and adhesive friction [30]. It is well documented that gray cast iron discs usually undergo abrasive friction [25,31]. One characteristic of abrasive friction is the breaking of bonds in both the pad material and the disc when they are brought into contact with one another. In other words, both the pad and the disk experience wear.

However, through the application of a dimpled surface, produced by PEA processing on the cast iron disc, a step change in brake performance is seen, and more significantly a transition to adhesive-like friction is observed. This is driven by the transfer layer development due to compaction galling. In this contact type and friction state, the pad materials were seen to transfer onto the surface of the treated disc, forming a compact, thin layer without any loss in friction performance. We can now translate this information to a friction mechanism model as in Fig. 6

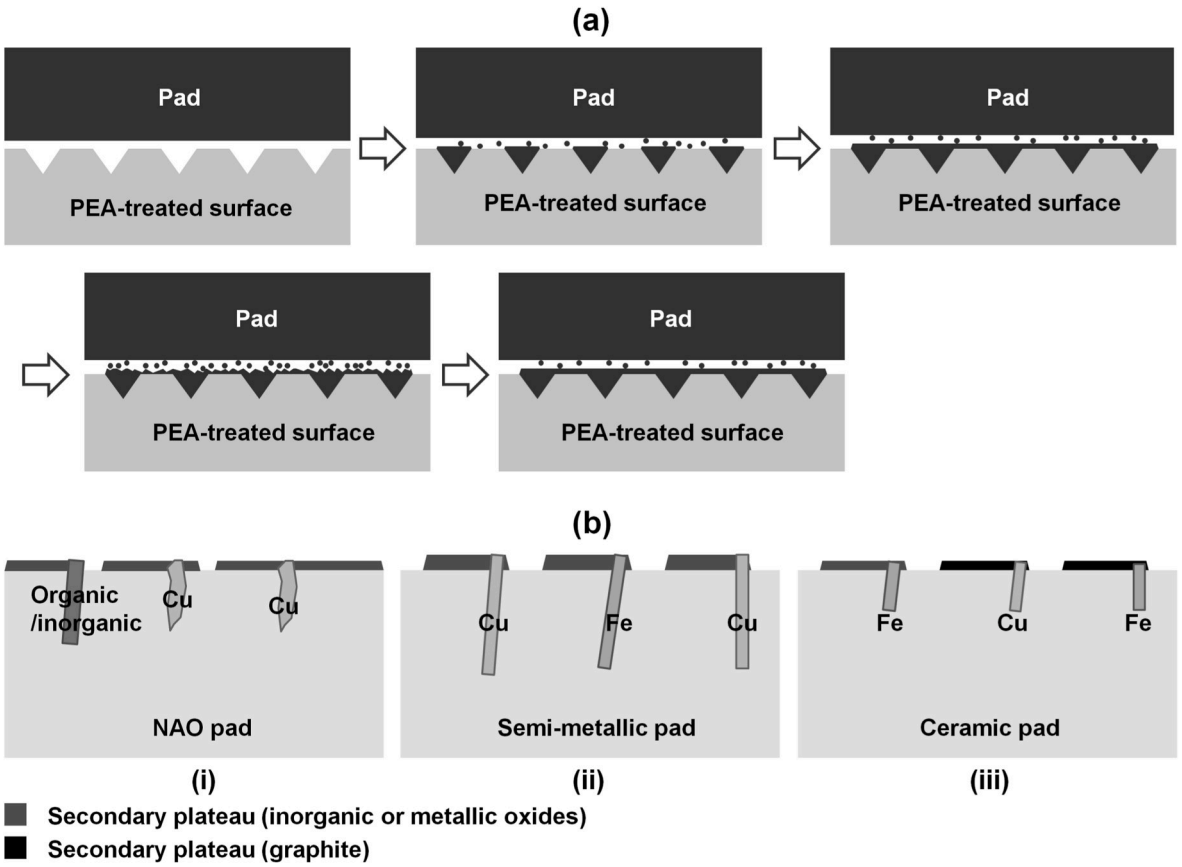

Fig. 6. (a) Friction process model with regards to PEA-treated cast iron brake discs; (b) the schematic of transfer layers on (i) the NAO pad, (ii) a semi-metallic pad, and (iii) a ceramic pad tested at low temperature.

wherein we show schematically the wear coupling. The wear debris – initially present as abrasive particles generated from the pad materials – fills firstly the dimples in the surface and other depressed areas and compacts to form a film as in compaction galling [27]. The transferred film then accumulates over the whole frictional surface and a transition away from abrasive friction mode occurs. The development of the transfer film, in turn means that both surfaces in the contact are effectively the same or similar materials. The friction generated in this contact is now achieved by rupture or shear of bonds identical to those in the pad material. As the film repeatedly accumulates and is worn off in this manner it leads to a relatively high and stable COF (Fig. 5a). When the secondary transfer layer reaches to a certain thickness, which is apparently developing over the first transfer layer anchored by the dimple-like disc surface, the formation and disruption of the friction layer would dynamically occur due to stress-induced cracks (Fig. 4c) and local spalling (Fig. 4d) of the secondary transfer layer mainly. It should be noticed that the thickness of the transfer layer seldom changed even though the test ran 1000 m sliding distance [25].

Fig. 6b–i is the schematic of tribo-film formation on the NAO pad where there is no obvious secondary plateau. The shapes of Fe and Cu are of small irregular pieces, instead of fibres as shown in Fig. 6b–ii and 6b–iii. The thin tribo-film comprises inorganic oxides which are partially from accumulated wear debris of the pad friction materials followed by the compaction and densification under the applied mechanical and thermal stresses.

A few researchers [32,33] have studied thermal spraying a WC-Co-Cr coating on brake discs and tested these against a low-metal pad. A typical contact plateau is found to form on the pad contact surface where the copper fiber acts as a primary plateau and worn materials from both the pad and the coating pile up and create a secondary plateau [1] as shown depicted in Fig. 6b–ii. A transfer layer is also generated from the pad onto the treated disc. The contact surfaces of both the pad and treated disc can accommodate worn material, which results in a relatively low wear rate and a low level of particle emissions. Their study also shows that it takes a longer time to reach steady state in temperature (from 25 to 150 °C) and COF (from 0.2 to 0.48) for the treated disc than untreated one during the PoD tests. At low temperatures (25–50 °C), the COF is 0.2, which is lower than the COF reported in this work. This could be due to transient effects in relation to the development of the transfer layer on the treated disc. Specifically, the transfer layer takes longer to build up on the WC/Co-treated disc than the PEA-treated disc. For a typical thermal spray, coating for anti-wear applications, high hardness and low porosity are desired for low wear of the disc on one hand. On the other hand, the dense and smooth coating likely makes the transfer layer uneven and nonuniform [32]. Contrary to the dense surface coating prepared by the thermal sparing technology, this work has proposed a different approach: utilize the dimple-like hard coating surface to provide firm mechanical interlocking anchor sites for the promotion of the quick formation of a transfer layer on the disc which leads to a shortening in the process of reaching a steady stage in COF even at the low or room temperature. The transfer layer prevents the treated disc from experiencing abrasive wear, and the results show almost no wear for the treated sample and much less wear for the counter pad.

The COF at low temperatures (or so-called cold friction performance) is quite dependent on the material composition of the secondary plateau on the pad contact surface. In previous research [25,34] where a ceramic pad instead of a NAO pad is used, the low COF level is due to formation of many carbon graphite patches as the secondary plateau at the low testing temperature (~25 °C), Fig. 6b–iii. Metallic oxides (Fe-Cu-Zn-O) would become the main composition of the secondary plateaus at high friction temperatures [32,35], which results in a higher COF at a level of

0.4–0.5 at elevated temperatures [32,33,36]. It is well-known that the friction performance of a ceramic pad is inferior in cold environments and superior at high operating temperatures, when compared to a NAO pad. Interestingly, the compaction galling-induced transfer layers on the treated discs in this and previous works [25] have no major differences in chemical compositions for those friction-decisive formulations, such as O, Fe, Cu, Zn and Mg [32,36]. The difference in COF at low temperature is mainly determined by the possible evolution in chemical compositions of the pad top surface during the sliding contact.

These insights also indicate not only the fact that it is highly desirable to generate a stable transfer layer by compaction galling, but also why there is a lack of formation of a stable transfer layer on the cast iron surface. This can be attributed firstly to the presence of free carbon (graphite), which, as mentioned previously, prevents material sticking [28]. Secondly, it can be attributed to the lack of dimples, to entrap third body wear debris developed during the wear process, which promotes compaction galling, as evidenced for the PEA coated surfaces.

This PoD study showed that, due to the initiation and evolution of compaction galling in the tribological contact, a PEA-treated disc exhibits negligible wear on its own surface and can result in up to 75% less wear of its corresponding brake pad. Also considering the wear debris from the PEA-treated disc can be as large as 200 μm in size, the PM emission would be less detrimental to human health, compared to the treated cast iron case. The PEA-treated disc thus represents a promising solution for reduction of both wear and non-exhaust emission of a brake system.

4. Conclusions

A dimple-like ceramic surface on cast iron brake disc can be generated by a PEA process. This dimple-like morphology provides a mechanical key for the initiation and growth of a transfer layer by compaction galling. The materials transferred from the friction materials of a brake pad first accumulate in the dimples and eventually result in a replenishable film over the entire frictional surface. As the transfer layer was anchored by the PEA-induced surface, the wear behavior of the brake disc and NAO pad changed away from abrasive. The result of this transition is that there was no wear observed on the PEA-treated sample. Furthermore, the pad materials also experienced significantly reduced wear when compared to standard brake disc material. In the boundaries of this investigation, we found that a PEA-treated cast iron shows a slightly higher COF than the variant without PEA treatment. This work therefore underlines the potential importance of a PEA-induced surface strategy for minimizing wear and in turn debris emissions in future brake systems. Further tests such as brake dynamometer tests will help confirm the validity of PEA applications in actual automotive brake systems.

Declaration of competing interest

The authors declare that they have no known competing financial interests or personal relationships that could have appeared to influence the work reported in this paper.

CRediT authorship contribution statement

Ran Cai: Formal analysis, Investigation, Data curation, Writing - original draft, Visualization. **Jingzeng Zhang:** Resources, Project administration. **Xueyuan Nie:** Conceptualization, Methodology, Validation, Resources, Writing - review & editing, Supervision. **Jimi Tjong:** Supervision, Funding acquisition. **D.T.A. Matthews:** Formal analysis, Writing - review & editing.

Acknowledgement

This research was supported by the Natural Sciences and Engineering Research Council of Canada. Thanks to Dr. S. Holger Eichhorn in the Department of Chemistry & Biochemistry, University of Windsor, for access to XRD instrument.

References

[1] T. Grigoratos, G. Martini, Brake wear particle emissions: a review, Environ. Sci. Pollut. Res. 22 (4) (2015) 2491–2504, https://doi.org/10.1007/s11356-014-3696-8.
[2] V.R.J.H. Timmers, P.A.J. Achten, Non-exhaust PM emissions from electric vehicles, Atmos. Environ. 134 (2016) 10–17, https://doi.org/10.1016/j.atmosenv.2016.03.017.
[3] M. Alemani, J. Wahlström, U. Olofsson, On the influence of car brake system parameters on particulate matter emissions, Wear 396–397 (2018) 67–74, https://doi.org/10.1016/j.wear.2017.11.011.
[4] M. Mathissen, J. Grochowicz, C. Schmidt, R. Vogt, F.H. Farwick zum Hagen, T. Grabiec, H. Steven, T. Grigoratos, A novel real-world braking cycle for studying brake wear particle emissions, Wear 414–415 (2018) 219–226, https://doi.org/10.1016/j.wear.2018.07.020.
[5] F.H. Farwick zum Hagen, M. Mathissen, T. Grabiec, T. Hennicke, M. Rettig, J. Grochowicz, R. Vogt, T. Benter, Study of brake wear particle emissions: impact of braking and cruising conditions, Environ. Sci. Technol. 53 (9) (2019) 5143–5150, https://doi.org/10.1021/acs.est.8b07142.
[6] M. Mathissen, T. Grigoratos, T. Lahde, R. Vogt, Brake wear particle emissions of a passenger car measured on a chassis dynamometer, Atmosphere (Basel) 10 (9) (2019) 556, https://doi.org/10.3390/atmos10090556.
[7] Mayor of London, London Environment Strategy Appendix 2: Evidence Base, Greater London Authority, London, 2018.
[8] Southern Ontario Centre for Atmospheric Aerosol Research (SOCAAR), Near-Road Air Pollution Pilot Study Summary Report Fall 2019, University of Toronto, Toronto, 2019.
[9] Department for Environment, Food and Rural Affairs, Scottish Government, Welsh Government, Department of the Environment in Northern Ireland, Non-exhaust Emissions from Road Traffic, Air Quality Expert Group, London, 2019.
[10] G.P. Ostermeyer, M. Müller, Dynamic interaction of friction and surface topography in brake systems, Tribol. Int. 39 (5) (2006) 370–380, https://doi.org/10.1016/j.triboint.2005.04.018.
[11] O. Aranke, W. Algenaid, S. Awe, S. Joshi, Coatings for automotive gray cast iron brake discs: a review, Coatings 9 (9) (2019) 552, https://doi.org/10.3390/coatings9090552.
[12] M. Federici, C. Menapace, A. Moscatelli, S. Gialanella, G. Straffelini, Effect of roughness on the wear behavior of HVOF coatings dry sliding against a friction material, Wear 368–369 (2016) 326–334, https://doi.org/10.1016/j.wear.2016.10.013.
[13] Y. Liu, Y. Wu, Y. Ma, W. Gao, G. Yang, H. Fu, N. Xi, H. Chen, High temperature wear performance of laser cladding Co06 coating on high-speed train brake disc, Appl. Surf. Sci. 481 (2019) 761–766, https://doi.org/10.1016/j.apsusc.2019.02.235.
[14] N.U. Rahman, L. Capuano, M.B.d. Rooij, D.T.A. Matthews, A. Garcia-Junceda, M. A. Mekicha, L. Cordova, G. Walmag, M. Sinnaeve, G.R.B.E. Römer, Laser metal deposition of vanadium-rich high speed steel: microstructural and high temperature wear characterization, Surf. Coating. Technol. 364 (2019) 115–126, https://doi.org/10.1016/j.surfcoat.2019.02.044.
[15] N.U. Rahman, M.B.d. Rooij, D.T.A. Matthews, G. Walmag, M. Sinnaeve, G.R.B. E. Römer, Wear characterization of multilayer laser cladded high speed steels, Tribol. Int. 130 (2019) 52–62, https://doi.org/10.1016/j.triboint.2018.08.019.
[16] T. Elbrigmann, Hard like diamond, Christophorus Porsche Magazine 384 (2017) 17.
[17] A.L. Yerokhin, X. Nie, A. Leyland, A. Matthews, S.J. Dowey, Plasma electrolysis for surface engineering, Surf. Coating. Technol. 122 (2–3) (1999) 73–93, https://doi.org/10.1016/S0257-8972(99)00441-7.
[18] Y. Nie, C. Kalapos, X. Nie, M. Murphy, R. Hussein, J. Zhang, Superhydrophilicity and antibacterial property of a Cu-dotted oxide coating surface, Ann. Clin. Microbiol. Antimicrob. 9 (2010) 25, https://doi.org/10.1186/1476-0711-9-25.
[19] T.W. Clyne, S.C. Troughton, A review of recent work on discharge characteristics during plasma electrolytic oxidation of various metals, Int. Mater. Rev. 64 (3) (2019) 127–162, https://doi.org/10.1080/09506608.2018.1466492.
[20] R. Cai, C. Zhao, X. Nie, Effect of plasma electrolytic oxidation process on surface characteristics and tribological behavior, Surf. Coating. Technol. 375 (2019) 824–832, https://doi.org/10.1016/j.surfcoat.2019.06.104.
[21] B.S. Lou, J.W. Lee, C.M. Tseng, Y.Y. Lin, C.A. Yen, Mechanical property and corrosion resistance evaluation of AZ31 magnesium alloys by plasma electrolytic oxidation treatment: effect of MoS2 particle addition, Surf. Coating. Technol. 350 (2018) 813–822, https://doi.org/10.1016/j.surfcoat.2018.04.044.
[22] X. Shen, X. Nie, J. Tjong, Effects of electrolytic jet plasma oxidation (EJPO) coatings on thermal behavior of engine cylinders, Heat Mass Transf. Und Stoffuebertragung. 55 (9) (2019) 2503–2515, https://doi.org/10.1007/s00231-019-02600-6.
[23] C. Zhao, W. Zha, R. Cai, X. Nie, J. Tjong, A new eco-friendly anticorrosion strategy for ferrous metals: plasma electrolytic aluminating, ACS Sustain. Chem. Eng. 7 (5) (2019) 5524–5531, https://doi.org/10.1021/acssuschemeng.8b06839.
[24] M. Federicia, M. Alemanib, C. Menapacea, S. Gialanellaa, G. Perriconeb, G. Straffelinia, A critical comparison of dynamometer data with pin-on-disc data

for the same two friction material pairs – a case study, Wear 424–425 (2019) 40–47, https://doi.org/10.1016/j.wear.2019.02.009.
[25] R. Cai, C. Zhao, X. Nie, Alumina-based coating with dimples as enabling sustainable technology to reduce wear and emission of brake system, ACS Sustain. Chem. Eng. 8 (2) (2020) 893–899, https://doi.org/10.1021/acssuschemeng.9b05302.
[26] K.M. Shorowordi, A.S.M.A. Haseeb, J.P. Celis, Velocity effects on the wear, friction and tribochemistry of aluminum MMC sliding against phenolic brake pad, Wear 256 (11–12) (2004) 1176–1181, https://doi.org/10.1016/j.wear.2003.08.002.
[27] J. Venema, J. Hazrati, D.T.A. Matthews, R.A. Stegeman, A.H. van den Boogaard, The effects of temperature on friction and wear mechanisms during direct press hardening of Al-Si coated ultra-high strength steel, Wear 406–407 (2018) 149–155, https://doi.org/10.1016/j.wear.2018.04.006.
[28] W. Österle, A.I. Dmitriev, The role of solid lubricants for brake friction materials, Lubricants 4 (1) (2016) 5, https://doi.org/10.3390/lubricants4010005.
[29] T. Grigoratos, M. Giorgio, Non-exhaust Traffic Related Emissions. Brake and Tyre Wear PM, JRC Science and Policy Reports, European Commission, 2014, pp. 1–53, https://doi.org/10.2790/21481.
[30] B. Hu, Friction and wear of automotive and aircraft brakes, in: G.E. Totten (Ed.), ASM Handbook, vol. 18, Friction, lubrication, and wear technology, ASM International, Materials Park, Ohio, 2017, pp. 969–982.
[31] A. Mohammadnejad, A. Bahrami, M. Goli, H. Dehbashi Nia, P. Taheri, Wear induced failure of automotive disc brakes—a case study, Materials 12 (24) (2019) 4214, https://doi.org/10.3390/ma12244214.
[32] J. Wahlström, Y. Lyu, V. Matjeka, A. Söderberg, A pin-on-disc tribometer study of disc brake contact pairs with respect to wear and airborne particle emissions, Wear 384–385 (2017) 124–130, https://doi.org/10.1016/j.wear.2017.05.011.
[33] C. Menapace, A. Mancini, M. Federici, G. Straffelini, S. Gialanella, Characterization of airborne wear debris produced by brake pads pressed against HVOF-coated discs, Friction (2019), https://doi.org/10.1007/s40544-019-0284-4.
[34] H. Jin, K. Zhou, Z. Ji, X. Tian, Y. Chen, L. Lu, Y. Ren, C. Xu, S. Duan, J. Li, S. en Hou, Comparative tribological behavior of friction composites containing natural graphite and expanded graphite, Friction (2019), https://doi.org/10.1007/s40544-019-0293-3.
[35] M. Eriksson, F. Bergman, S. Jacobson, On the nature of tribological contact in automotive brakes, Wear 252 (1–2) (2002) 26–36, https://doi.org/10.1016/S0043-1648(01)00849-3.
[36] Y. Lyu, M. Leonardi, J. Wahlström, S. Gialanella, U. Olofsson, Friction, wear and airborne particle emission from Cu-free brake materials, Tribol. Int. 141 (2020) 105959, https://doi.org/10.1016/j.triboint.2019.105959.